STUDY OF STABILITY OF ZnO NANOPARTICLES AND GROWTH MECHANISMS OF COLLOIDAL ZnO NANORODS

A Thesis

by

KWANG JIK LEE

Submitted to the Office of Graduate Studies of
Texas A&M University
in partial fulfillment of the requirements for the degree of

MASTER OF SCIENCE

August 2005

Major Subject: Mechanical Engineering

STUDY OF STABILITY OF ZnO NANOPARTICLES AND GROWTH MECHANISMS OF COLLOIDAL ZnO NANORODS

A Thesis

by

KWANG JIK LEE

Submitted to the Office of Graduate Studies of
Texas A&M University
in partial fulfillment of the requirements for the degree of

MASTER OF SCIENCE

Approved by:

Chair of Committee,	Hung-Jue Sue
Committee Members,	Jaime Grunlan
	Michael A. Bevan
Head of Department,	Dennis O'Neal

August 2005

Major Subject: Mechanical Engineering

ABSTRACT

Study of Stability of ZnO Nanoparticles and Growth Mechanisms of

Colloidal ZnO Nanorods. (August 2005)

Kwang Jik Lee, B.S., Korea University

Chair of Advisory Committee: Dr. Hung-Jue Sue

After hydrolyzing zinc acetate in methanol solution, spherical ZnO nanoparticles in the size range from about 2.5 to 5 nm were synthesized by maintaining a ZnO concentration of 0.02M. Compared to ZnO nanoparticles prepared via other methods, the particles prepared using our novel colloidal chemistry exhibit narrow size distribution and a high sensitivity to the surrounding environment. The structure and composition of the white powders precipitated from the colloidal solution can vary, depending on how the powder samples are prepared. Factors such as desorption and adsorption of methanol, binding of water and exposure to humid air have been studied to correlate to the structure and composition observed from the precipitated powder. Methanol desorption rate and excess KOH on the particle surface have played an important role in the structural changes. Furthermore, upon annealing, the white precipitate is recovered to wurtize ZnO. XRD and TEM are used to study the structural transformation of ZnO nanoparticles.

Using the zinc oxide spherical colloidal solution, ZnO nanorods could be grown after increasing the initial concentration of the precursor solution using two different approaches. Nanorods grown can form at ZnO precursor concentrations as low as 0.04 M. Three distinct growth stages are observed during the formation of ZnO nanorods. In the early stages of growth, ZnO nanorods show high uniformity with less than 5 nm in diameter and have an aspect ratio of less than 10. At the final stage of growth, ZnO nanorods grow randomly in all dimensions, resulting in sizes over 10 nm in diameters, which leads to a large reduction in aspect ratios.

The growth mechanisms of ZnO nanorods are related to precursor concentration, surfactant, aging time, and temperature. In addition, upon annealing, further growth of ZnO nanorods is observed. Approaches for size and shape control of ZnO nanocrystals are discussed.

ACKNOWLEDGMENTS

I would like to first and foremost give all the glory to God who, without Him and the tremendous grace and mercy He has shown me throughout my life and throughout this research, none of this would have been possible. Even looking back, I know that I did not and could not have done this in my own strength (2 Cor. 12: 9).

"Then Samuel took a stone and set it up between Mizpah and Shen. He named it Ebenezer, saying, "Thus far has the LORD helped us." (Samuel 1. 7:12). I have no doubt that the confession of faith above will be kept throughout my life.

I thank my family, especially my parents, uncle and aunt, who have supported my career and through warm guidance led me to be what I am now. Their constant love, support, encouragement and challenging will without a doubt establish a firm foundation on which I can develop my effort and knowledge to achieve my final goal of obtaining a Ph.D.

I would like to thank my advisor, Dr. H.-J. Sue. Due to his high expectations, I was able to grow more independent. Without his guidance, none of the accomplishments achieved during my studies could have been possible. A special thanks goes to the former advisors at KIST (Korea Institute of Science and Technology) for their consideration enabling me to perform some of my research in Korea during the summer of 2004.

Also, I would like to thank all my friends and a minister at Vision Mission Church in College Station. Their warm hospitality and companionship relieved me from the fright of first living in a foreign country and helped me sustain an intimate relationship with God.

Lastly, I would like to thank all my group members. I hope to keep in close touch with all the members even after leaving College Station and wish all the best of luck and success throughout their careers.

TABLE OF CONTENTS

Page

Page

LIST OF FIGURES

FIGURE Page

FIGURE Page

FIGURE Page

LIST OF TABLES

1. INTRODUCTION

1.1 Research on nanometer-sized materials

Research on nanometer-sized materials has increased remarkably during the past years due to their unique characteristics termed quantum confinement effects as well as therefore potential applications. The term, quantum confinement effect, was introduced to explain a wide range of mechanical, electrical and optical properties of nano-sized materials in response to changes in dimensions or shapes within nano-scales [1-5]. For example, CdSe nanocrystals show changes in color in the range of the visible spectrum, while confinement effects in ZnS appear in the ultraviolet region. Similar findings are also observed with ZnO nanoparticles, exhibiting red shifts of the UV-Vis absorption peaks for the particles less than 7 nm in size [6].

1.2 ZnO nanoparticles

ZnO with a wide band-gab (3.27 eV) in bulk is one of the semiconductor materials, making it attractive for the nano electronic and photonic applications. Its advantages over other materials for electronic applications lie in a high exciton binding energy (60 meV), breakdown strength and its multifunctional (piezoelectric, ferroelectric and

---

This thesis follows the style of *Nano Letters.*

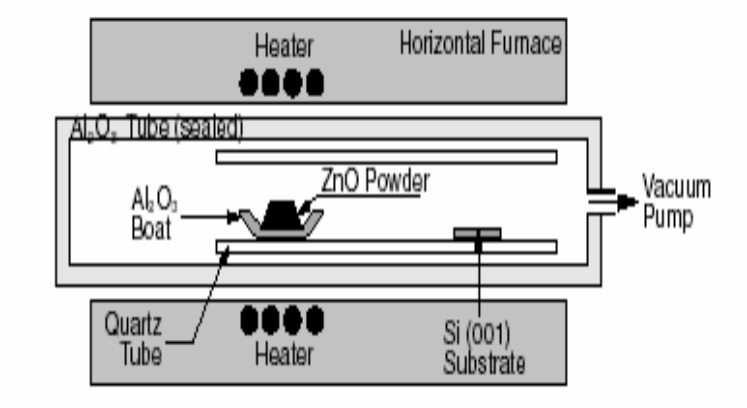

Figure 1.1. Diagram of the experimental set up for the evaporation method [9].

ferromagnetic) [7, 8]. In addition, ZnO is much more resistant to radiation damage than other common semiconductor materials, such as Si, GaAs and CdS. The applications of ZnO to the UV-emitting diodes, cathode-ray phosphors, transparent conductor, varistors, chemical sensors, UV-protection films, and ultrafast nonlinear optical devices have been performed [8]. To prepare ZnO nanoparticles or thin films, several methods such as chemical vapor deposition, molecular beam epitaxy, metal organic vapor-phase epitaxy, spray pyrolysis and wet-chemistry colloid preparation have been developed. Wet-chemistry approaches, as opposed to other methods requiring expensive and complicated processes (Fig. 1.1), have their own attractiveness in that ZnO nanoparticles can be synthesized with easy, low cost and without specific equipments. This method was first reported by Spanhel and Anderson [10] and then modified and extended at several points to simplify the procedures. With these wet-chemistry approaches, high concentrated ZnO nanoparticles in the size range 2 to 7 nm in colloidal solution can be prepared.

1.3 Barriers to overcome in wet-chemistry approaches

1.3.1 Insufficient knowledge of ZnO growth kinetics and mechanisms

For the ZnO nanoparticles prepared via wet-chemistry approaches, there are still several obstacles to overcome for further applications. First of all, a fundamental understanding of the ZnO growth kinetics as well as mechanisms is still not enough to provide precise knowledge in controlling the dimensions and shapes of the particles. It is already known that thermodynamic behavior of nanoparticles is different from that of the bulk materials

due to their significantly increased free energy term ΓA (the product of the surface free energy and surface area) [11, 12]. However, since ZnO nanoparticles are too sensitive to the environmental conditions such as binding of water, absorption and desorption of solvent, pH changes, exposure to air, it's not easy to predict exactly their final status. Therefore, new wet-chemistry approaches are required to obtain an exact knowledge of the growth process of nanocrystals in other to control their sizes, size distribution, shapes and structures under several different experimental conditions. A new wet-chemistry method of synthesizing ZnO nanoparticles were reported by our group [13]. Colloidal ZnO nanoparticles were prepared via our unique wet-chemistry approach from which nanoparticles were obtained in a transparent methanol solution within 5 min. In this new method zinc acetate powders, as opposed to other synthetic methods reported in somewhere, were added directly into the KOH/Methanol solution accompanying the formation of ZnO nanoparticles. This method is not only a simple and easy way to handle but also provides more choices of base and alcohol mixture such as KOH, NaOH, LiOH, methanol, ethanol and isopropanol. The quantum confinement effect, red shifts of the UV-Vis absorption peaks in response to the increase of particle size bellow 7 nm, was observed from both of the ZnO nanoparticles and nanorods prepared based on this new method [14].

White precipitants were obtained from the colloidal ZnO solution above. The structure of the precipitant changed according to surface conditions due to its high sensitivity to surface environments. ZnO nanorods grown from the same colloidal solution also show unique properties such as high uniformity and narrow in width [14]. This new synthetic

method will be introduced and the reasons why and how this new wet-chemistry leads to such interesting results will be discussed in more detail in the following chapters. The main subjects of this research, therefore, are the following; 1) study the surface environments causing changes in structures of ZnO nanoparticles and 2) establish the growth kinetics and mechanisms of ZnO nanorods grown via our new chemistry approach.

1.3.2 Surface defects of ZnO nanoparticles

Surface passivation and functionalization of ZnO nanoparticles are also a matter of great importance due to its surface defects [15]. The luminescent properties of undoped ZnO quantum dots vary depending on the various stabilizing agent used for capping and surface treatments. Though well known as a UV-emitting (~ 320 nm) material, ZnO nanoparticles emit green light (~ 500 nm) (Fig. 1.2) because of the defects on the surfaces of nanoparitcles. It is reported that the green emission of the ZnO nanoparticles results from the existence of oxygen vacancies or the zinc interstitials on the particle surfaces [15]. Furthermore, when a thin layer of $Zn(OH)_2$ covers the surface during the wet-chemical synthesis, the exciton transition is quenched [16].

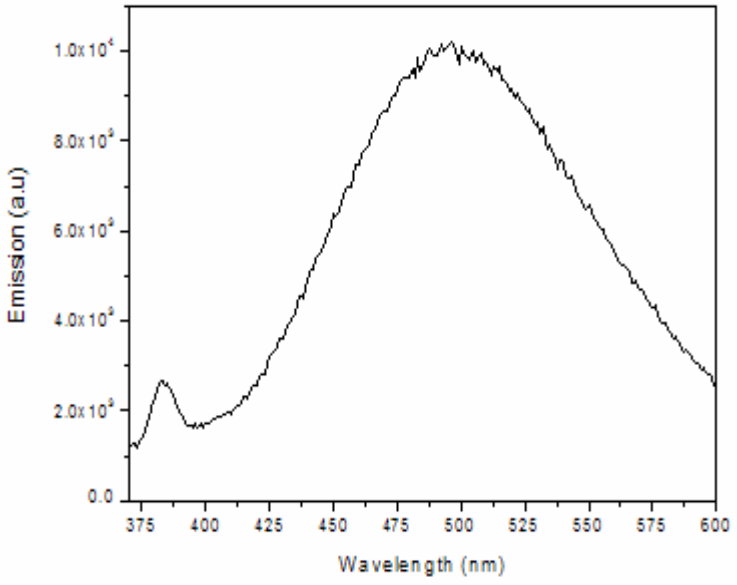

Figure 1.2. The photoluminescence (PL) spectrum of ZnO nanoparticles which shows both UV and visible emission peaks.

To enhance ultraviolet emission while decreasing green emission, several surface treatments such as hydrogen plasma treatment, chemical doping and annealing have been reported [15-17]. Quenching of the green luminescence complemented by the enhancement of the UV luminescence was observed after hydrogen plasma treatment on ZnO [15]. Strong UV emission is also obtained from ZnO quantum dots after annealed at high temperatures (higher than 125°C) as the surface $Zn(OH)_2$ is released [16]. The copper doping in ZnO quantum dots also showed quenching of green emission [15]. PVP-capped ZnO quantum dots have been widely studied [15, 16]. Capping of ZnO nanoparticle surfaces by using poly(vinyl pyrrolidone) (PVP) also exhibited enhanced UV photoluminescence and reduced green emission of ZnO nanoparticles [17]. This is attributed to the nearly perfect surface passivation of the ZnO nanoparticles by the PVP molecules. For the ZnO nanoparticles prepared via our new wet chemistry method, the optimal molar ratios of Zn(II)PVP= 5:6, as opposed to the value of 5 to 3 in the reference [17], was obtained from the PL experimental results (Fig. 1.3). For electronic applications, however, PPV material is not suitable for the capping materials due to its insulating property. Therefore it is an urgent matter to find new materials and techniques for the passivation and functionalization of ZnO nanoparticles.

1.3.3 Dispersion of ZnO into the polymer matrixes

Nanocomposites based on polymers are a new class of composites that are particle filled polymers for at least one dimension of these particles is in the nanometer range. The key to nanocomposites is the ability to either partially or completely separate the individual

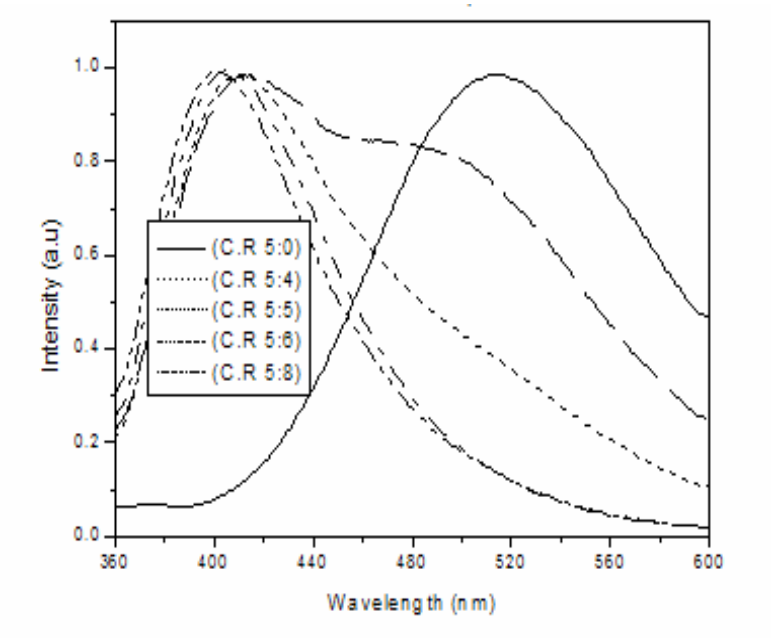

Figure 1.3. Photoluminescence spectra of the PVP capped ZnO nanoparticles. The optimal molar ratios of Zn(II)/PVP= 5:6 is shown.

nanofillers (intercalate or exfoliate) and make them miscible in polymers such as PP, PET and PVA (Fig. 1.4). However, since the enormously increased surface free energy caused by large surface/volume ratio of particles in this regime, leading to aggregations of nanoparticles, it's not easy to achieve fully exfoliated or intercalate polymer nanocomposites. A lot of researchers these days focus their research activities on solving the problem of aggregations of nanoparticles and therefore achieving fully exfoliated polymer nanocomposites. Compared to the conventional composite materials, when fully exfoliated, polymer nanocomposites show highly improved electrical, optical, mechanical properties [1-5] such as increased mechanical strength, improved gas barrier property, higher heat and wear resistance and enhanced efficiency of the electronic devices. The pictures shown in Fig 1.5 are the optical microscopy images of a neat epoxy panel and α-zirconium phosphate-epoxy nanocomposites prepared by intercalation with surfactant followed by exfoliation. Though the same amount of nanofillers was added into the polymer epoxy panel, the pictures clearly show the differences in optical properties. Optical properties of the polymer nanocomposites vary depending on the degree of exfoliation/dispersion of nanofillers in polymer matrixes. Because the size of nanoparticles is less than the wavelength of visible light, when well dispersed, fully exfoliated polymer nanocomposites can be clear. The transparent α-zirconium phosphate-epoxy nanocomposites could be obtained after exfoliating of nanofillers by using a surface modifiers.

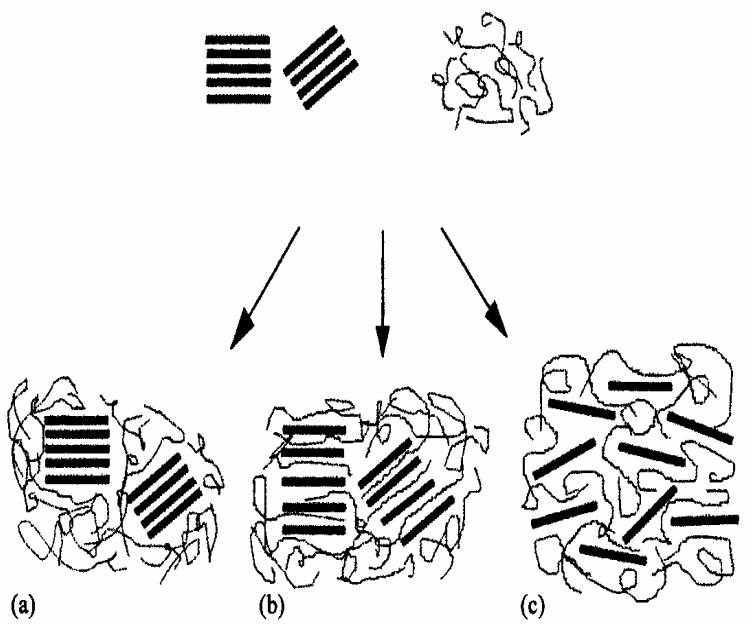

Figure 1.4. Layered silicate and polymer composites. a) phase separation, b) intercalated, c) exfoliated [18].

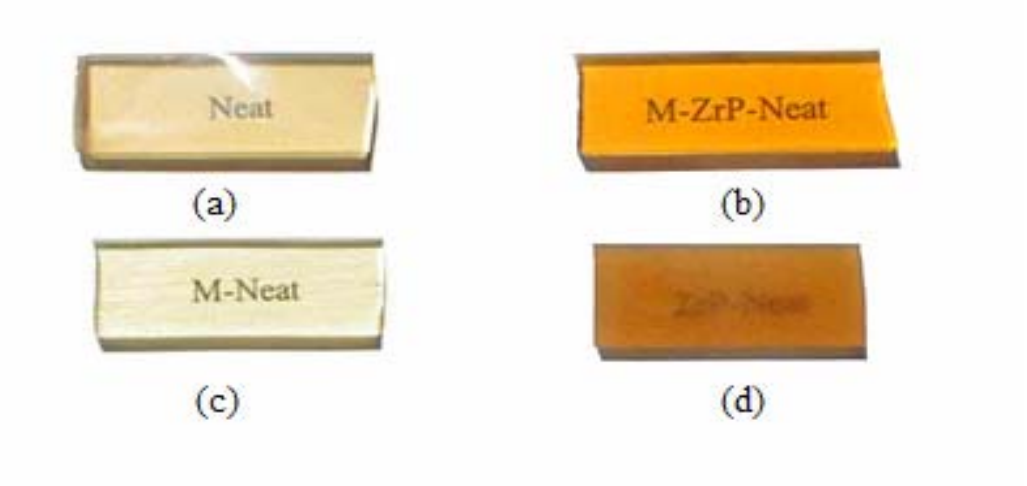

Figure 1.5. Optical microscopy images. (a) neat epoxy, (b) exfoliated (surface modified) ZrP/epoxy nanocomposite (c) surface modifier added neat epoxy, (d) ZrP+epoxy (pristine α-ZrP, 2 vol%).

Dispersions of nanoparticles into the polymer matrices is critical points to electrical applications, especially hybrid LEDs (light-emitting diodes) consisting of semiconducting polymers and inorganic nanoparicles. No light was emitted from the ZnO nanoparticles in the devices due to their aggregation. It is thought to be the result of self-quenching, quenching of an excited atom or molecular entity by interaction with another atom or molecular entity of the same species in the ground state [19]. Therefore, developing of new technologies such as self-assembled monolayers (SAMs) to disperse nano-sized materials uniformly in the polymer matrixes is of a matter of great importance. The main key of realizing nanotechnology for the actual applications in industries in near future may lie in how to disperse/exfoliate nanoparticles.

2. LITERATURE OVERVIEW

2.1 Research on nanometer-sized materials

Research activities on the fabrication of nanometer-sized functional materials, such as semiconductor quantum dots, tubes, and wires, have increased enormously because of their attractive size and shape dependent electrical and optical properties [1, 2]. For example, high aspect ratio CdSe nanocrystals have been reported to show greatly enhanced quantum efficiency in photovoltaic devices by forming interpenetrating network (IPN) structures (Fig. 2.1) [20]. These nano-sized phenomena, referred to as "quantum confinement effect", are of significant interest from both fundamental and technological points of view.

So far, most research on size and shape control of nanocrystals in the colloidal solution has been focused on CdSe, CdS and Co [21-24]. To study the behavior of the nanoparticles and explain the growth process of these nanocrystals from the quantum dots to nanorods, several theories and mechanisms are suggested. Furthermore, important factors affecting the structure, size and shape of the nanoparticles such as surface environment, surfactant composition, time variation of monomer concentration and temperature are reported.

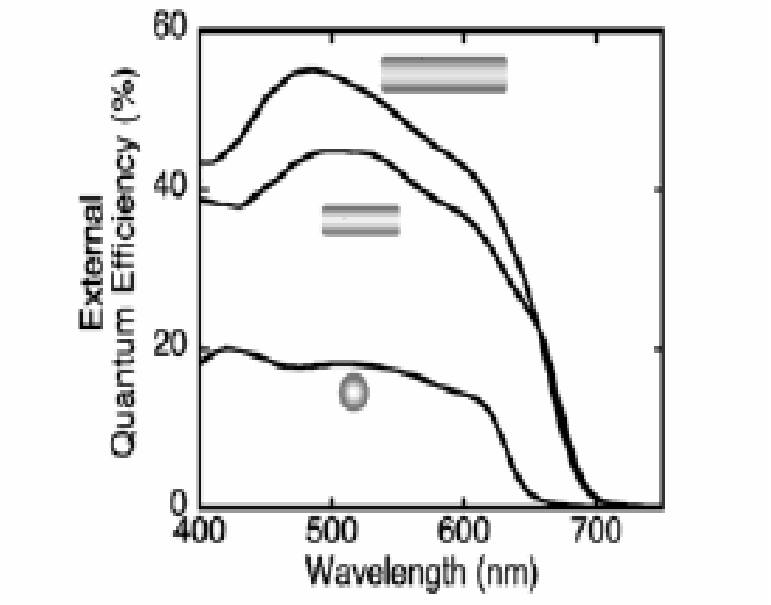

Figure 2.1. Enhanced external quantum efficiencies of the hybrid photovoltaic devices. 7-nm-diameter CdSe nanorods with lengths of 7, 30, and 60 nm were used [20].

2.2 Thermodynamic behavior of nanoparticles

The thermodynamic behavior of small particles has been studied [11, 12]. It is reported that the changes in phase stability complemented by decreasing particle size results from the differences in interfacial free energies of the surfaces of polymorphs of the same materials. The surface role to the total energy grows significantly as the particle size decrease due to the highly increased free energy term γA (the product of the surface free energy and surface area). The difference in surface energy of nano-sized materials can also favor the formation of a particular polymorph [12]. For example, though corundum, α-Al_20_3, is the thermodynamically stable phase of coarsely crystalline aluminum oxide, syntheses of nanocrystalline α-Al_20_3 usually results in γ-Al_20_3. Similar results were found the synthesis of nanocrystalline cubic $BaTiO_3$, tetragonal ZrO_2, tetragonal ZrO_3 and monoclinic Y_2O_3 [25-27]. The results are attributed to the fact that these metastable structures are favored to lower the total energy of the material by decreasing in surface energy.

2.3 Surface environment affecting the structure of nanoparticles

Reversible surface-controlled structure transformations in nanoparticles are observed [28, 29]. Here nanoparticles undergo structural changes in response to the changes in the surface environments rather than particle size. Differences in surface environments due to water binding, surface-bound ligand, changes in pH or ionic strength can cause changes in surface free energy of nanoparticles in solution, leading to the internal

structural transformation [28]. The effect of pH changes on the yield of ZnO nanoparticles is already studied by using our new wet-chemistry approach (Table 2.1) [13]. It is also reported that changes in the aggregation state can induce reversible internal structural transformations in ZnS nanoparticles suspended in methanol [28]. Dispersed or weakly aggregated ZnS nanoparticles in suspension showed a more distorted internal structure than strongly aggregated nanoparticles.

The structure transformation of ZnS nanoparticles also occurred when methanol solvent was desorbed or reabsorbed [29]. Furthermore, significant structural modification was caused when adding water into the colloidal solution at room temperature, reducing distortions of the surface and interior to generate a structure close to that of sphalerite (tetrahedrally coordinated cubic ZnS) [29]. These findings indicate that the structures of nanoparticles can be modified by controlling particle surface conditions even after synthesis. In addition, changes in nanoparticle structure could be used as principles of sensors which can monitor the changes of water, methanol in air in term of the structural transformations.

2.4 Theory of ‘Focusing’ and ‘Defocusing’ (CdSe)

The focusing and defocusing theory was suggested to explain the growth process of CdSe nanocrystals from the quantum dots to nanorods [21]. Under the thermodynamic condition, spherical shape of materials is favored at the beginning of the reaction due to their minimum surface areas versus the same volume, resulting in minimum (stable)

Table 2.1. The pH values of solutions with various concentrations of zinc acetate dehydrate and KOH. Initial pH value is KOH/MeOH solution without zinc acetate dihydrate.

Concentration		pH (initial)	pH (5min)	pH (2h)	ZnO nanoparticles
Zinc acetate	KOH				
0.01 M	0.02 M	12.07	8.58	8.45	Yes
0.02 M	0.04 M	12.24	9.60	8.77	Yes
0.015 M	0.04 M	12.24	10.83	10.69	No
0.01 M	0.04 M	12.24	11.74	11.62	No
0.20 M	0.40 M	13.33	9.10	8.81	Yes

energy states. Therefore, spherical shape of nanocrystals forms at the beginning of the reaction. However, it is found that size distribution of these nanoparticles varies according to monomer concentration. At high monomer concentration, all particles grow regardless of size and the smaller particles grow faster so that CdSe nanocrystals with nearly monodisperse in size are observed (Focusing). However, at low monomer concentration, small particles are depleted as larger ones grow, leading to broad size distribution (Defocusing). So these separate stages are defined and termed as 'focusing' and 'defocusing', respectively.

2.5 Three different stages in the shape evolution (CdSe)

Mechanisms for the rod formation of the CdSe nanocrystals also have been reported to consist of three separate stages, depending on the monomer concentrations [22]. The experimental results revealed that at high monomer concentration, nanocrystals grow exclusively along the c-axis of the wurtzite structure. At intermediate monomer concentration, however, nanocrystals grow simultaneously in three dimensions. At low monomer concentration, the aspect ratio decrease in a process as a result of both the previous stage and intraparticle diffusion on the surface of the nanocrystals. In this final stage it is noted that the intraparticle diffusion is different from normal Ostwald ripening because it occurs at lower monomer concentration and by monomer migration from small to larger ones.

2.6 Selectively binding of surface ligands

It is also reported that changes of the monomer concentration by adding strong cadmium ligands, such as hexylphosphonic acid or tetradecylphosphonic acid, would enable the control of the shapes as well as the dimensions of the CdSe nanocrystals [23]. In addition, surfactant composition plays an important role in controlling the growth rates of different faces by dynamically coating the particles with a close packed monolayer. The growth can be modified through charge transfer, followed by the surface tension is lowerd [23].

The synthesis of shape-controlled CdSe nanocrystals was reported by Manna et al [24]. They revealed that a wide variety of shapes of CdSe nanocrystals, such as rods, teardrops, tetrapods, and branched tetrapods, could be synthesized simply by varying surfactant composition, time, and monomer concentration. Magnetic cobalt nanorods having two- and three-dimensional superstructures have also been prepared in the similar ways to those of CdSe nanocrystals [23].

2.7 Research on ZnO nanoparticles and nanorods

Nano-sized ZnO colloids were first prepared by hydrolyzing highly diluted zinc acetate about 0.001 M in an isopropanol solution [30], and highly concentrated ZnO colloidal solutions about 0.1 M were later prepared using sol-gel synthesis [10, 31]. A few modifications have been made on this method, making this synthetic process simpler and

easier to handle. [31, 32]. For example, the colloidal ZnO solution was prepared by the addition of basic solution (0.03 M solution of KOH (65 ml)) to a zinc acetate alcoholic solution (zinc acetate dehydrate (0.01 M) in methanol (125 ml)) under vigorous stirring for 2 h at about 60 °C [32].

It has been reported that rod-shaped ZnO was obtained after concentrating of the precursor solution prepared in the same way described above and aging it for different lengths of time [32]. ZnO nanorods having a diameter of about 15 nm could be grown at a high concentration of about 0.1 M upon evaporating the spherical ZnO nanoparticle precursor solution at an initial concentration of 0.01 M. Similar observations were reported by Verges et al. for the formation of rodlike microcrystals [33].

In the above studies, it has been concluded that, to grow ZnO nanorods, it is necessary to increase the ZnO concentration in the precursor solution at 60 °C or higher. As for the mechanisms for the growth of ZnO nanorods, “Ostwald ripening” and “oriented attachment” were proposed to explain the formation of ZnO nanorods [30]. In here, ‘oriented attachment’ was proposed for the first time by Penn and Banfield to describe the coalescence of anatase and iron oxide nanoparticles under hydrothermal conditions. After that, oriented attachment was used to explain the crystal growth of TiO_2 and formation of rodlike ZnO microcrystals. This can be shown from the high resolution TEM (HRTEM) pictures, revealing almost perfectly alignment of crystalline lattice planes or dislocation at the contact areas between the adjacent particles (twin structure).

However, it is uncertain whether or not the proposed growth mechanisms depicted above can be applied to ZnO nanorod growth under other conditions.

The ZnO quantum dots and nanorods to be reported in following chapters were synthesized and grown via a new wet-chemistry route at low precursor concentrations [13]. The ZnO colloidal solutions and nanorods above show unique properties compared to those of ZnO prepared by using other methods. Based on the results above, new mechanisms will be proposed to describe the growth of the ZnO from the quantum dots to nanorods. Transmission electron microscopy (TEM), X-ray diffraction (XRD) and UV-Vis spectrophotometer were used to analyze the ZnO nanorods structure, size, and optical absorption characteristics.

3. EXPERIMENTAL

3.1 Materials

Zinc acetate dehydrate ($Zn(OAc)_2 \cdot 2H_2O$) was obtained from Fluka. KOH and micro-sized ZnO powder having 99.9 % purity were purchased from Aldrich. Here micro-sized ZnO powder was used as a control sample. Methanol with reagent grade of 99.9 % purity was used.

3.2 Synthesizing of a colloidal ZnO solution

A new wet-chemistry was employed to prepare colloidal ZnO solutions. First, 0.04 M KOH solution in methanol was prepared by adding 0.224 g KOH into 100 ml methanol. After sonicating the solution for 5 min, it was heated up until the final temperature reaches around 55 °C under stirring and refluxing in an oil bath. To adjust the reaction stoichiometry of zinc acetate dehydrate and KOH of 1 to 2 (0.02 M to 0.04 M), 0.439 g of Zinc acetate dehydrate ($Zn(OAc)_2 \cdot 2H_2O$) powder was added into the solution. Within 5 min, transparent ZnO colloidal solution was obtained. To study the growth process and mechanism of ZnO particles, the solution was aged for several days under the same conditions.

3.3 Precipitation and surface environments of white powders

During the aging process of the transparent ZnO colloidal solution, the change in colors of the solution from transparent to cloudy occurred after two-day aging, followed by the precipitation of white powder on the bottom of the flask. To identify the white precipitants, both XRD and TEM were utilized and each result was compared. It is also known that nanoparticles are highly sensitive to surface environments such as water, moisture, humidity, pH and solvents [28, 29]. Experiments were designed to study which factors are responsible for the structural and morphological changes of ZnO nanoparticles in our new synthetic system. The experimental conditions are summarized as follows.

ZnO sample preparations under different environmental conditions;

Each solution below was used as a precursor solution.

- Transparent ZnO colloidal solution
- Opaque ZnO colloidal solution

Precursor solutions were prepared based on our new wet-chemistry approach explained in detail on the previous page.

3.3.1 Drying conditions of white precipitants in methanol

Several approaches were employed to get powder form ZnO under different drying conditions.

- Slow evaporation of opaque ZnO colloidal solution
- Fast evaporation of opaque ZnO colloidal solution in the dry atmosphere
- Fast evaporation of opaque ZnO colloidal solution in the humid atmosphere
- Decantation of methanol solution after centrifuging

To obtain a slowly evaporated sample, opaque colloidal solution opened into air in a glass beaker at room temperature. Cloudy solutions turned to be transparent soon during the slow volatilization of MeOH, indicating that nanoparticles redispersed into the methanol solution. Further evaporation of MeOH allowed white powder to reprecipitate and then after the precipitant was just left in the open air. Quick volatilization of methanol solution was done by pouring the same colloidal solution onto the spacious weighing paper. The large contact area between the solution on the paper and air allowed that white powders form within a one day. However, the final state of the samples was a little bit different in this approach, depending on the humidity of the atmosphere. The completely dried precipitant was obtained under the dry and cool air. However, in the humid atmosphere, precipitants remained in a little bit wetted state even after evaporation of MeOH. The most freshly prepared white powder sample was obtained after centrifuging and decanting the opaque ZnO colloidal solution. To minimize other effects such as exposure of the particle to air, the sample was quickly examined with XRD.

3.3.2 Effects of the annealing

The white precipitant prepared via a slow evaporation method was annealed at 130 °C for different lengths of time (30 min, 1 hours, 3 hours) to track its structural and morphological transformation at high temperature. To monitor each stage, both TEM and XRD were used.

3.3.3 Effects of water contents

Distilled water was added into the opaque ZnO colloidal solution and ZnO powder, respectively.

- Distilled water into the opaque ZnO colloidal solution
- Distilled water into the ZnO powder

The ZnO powder used here was obtained after 3-hour annealing of the white precipitant at 130 °C. Water added opaque ZnO colloidal solution was just left on the table at room temperature for 3 days. The remnant liquid was decanted after centrifuging the solution mixture to get powder samples. ZnO powder in which distilled water was added was also prepared under the same condition with that of the water added opaque ZnO colloidal solution. The ZnO powder was taken out to take XRD.

3.3.4 Effects of methanol readsorption

All the experimental conditions are the same as the previous one (water added to ZnO) except that here methanol was used instead of water.

3.3.5 Effects of pH

The value of pH was recorded with some solution samples above.

3.4 Preparation of ZnO nanorods

The ZnO colloidal solution above was used as a precursor solution to grow ZnO nanorods. Since it has been shown that an increase in ZnO concentration in the precursor solution is necessary to grow from quasi-spherical shaped ZnO nanocrystals into nanorods, two approaches were undertaken to increase the concentration of the starting precursor sol with an initial concentration of 0.02 M. One approach was to use a Rotavapor to rapidly increase the concentration of precursor solution at 55 °C. This solution was then aged at 55°C for 12 hours under refluxing and stirring in an oil bath. The other approach was by conducting a 10-day of reflux of the precursor solution at 55 °C by slow evaporation of solvent via a small cap opening until the final concentration reaches ~ 0.04 M. Meanwhile, the evaporation rate of the colloidal

solution was recorded at various lengths of time to determine how the concentration influences the nanorod growth mechanisms.

To study how other processing parameters affect the formation of ZnO nanorods, syntheses were also performed under different temperatures, precursor concentrations, evaporation rates and aging times. In addition, ZnO nanorods grown here were annealed at 110 °C for 3 hrs in an oven to observe further growth of ZnO nanorods. For clarity, all the experimental conditions performed in this research are summarized in Table 3. 1.

3.5 Characterization of structure and optical properties

To study the ZnO nanorod crystal structure, X-ray diffraction (XRD) using a diffractometer (Bruker D8 Advanced Powder X-ray Diffractometer) with Cu-K_α incident radiation was utilized. For XRD experiments, powder samples were used.

The size and shape of the ZnO nanoparticles were determined using a JEOL 2010 high resolution transmission electron microscope (HRTEM). The TEM microscope has a spatial resolution of 0.23 nm when operating at 200 keV. The structure of the ZnO nanoparticles was also studied by electron diffraction. TEM samples were prepared by evaporating a drop of colloidal suspension on copper grids and then dried in a vacuum desiccators for at least two hrs. Optical absorption spectra were also recorded on a HP 8451 diode array spectrophotometer. A bulk (micro-sized) ZnO powder purchased from

Table 3. 1. A summary table showing the formation of ZnO nanocrystals as a function of temperature, precursor concentration, evaporation rate and aging time. All shapes of ZnO nanocrystals were confirmed by TEM observations.

Preparation of the Precursor Solution [11] Spherically Shaped ZnO Nanoparticles							
Temperature		55°C	55°C	55°C	55°C	45°C	Room T.
Precursor Con		0.02 M	0.02 M	0.02 M	0.2 M	0.02 M	0.02 M
Evaporation Rate		Quickly	Slowly	0	Slowly	Slowly	Slowly
Aging Time (Final Con.)	2 hr.	Spherical (0.1 M)					
	12 hr	Rods (0.1 M)			Rods (1day, 0.2M)		
	7 days		Spherical (~0.03 M)				
	10 days		Rods (~0.04 M)	Spherical (0.02 M)		Rods (17days,~0.04 M)	
	21 days						Spherical (~0.1 M)

Aldrich was dissolved in Methanol to take UV–Vis spectra and then compared with those of ZnO nanoparticles and nanorods.

4. STABILITY OF ZnO NANOPARTICLES

4.1 UV-Vis and PL characterization of ZnO nanoparticles

After hydrolyzing zinc acetate in methanol solution, spherical ZnO nanoparticles in the size range of about 2.5 to 5 nm were synthesized by maintaining a ZnO concentration at 0.02M [13]. This new wet-chemistry approach allows ZnO nanoparticles to be obtained in a transparent colloidal solution within 5 min. To characterize the colloidal solution, both UV-Vis and photoluminescence (PL) spectra were taken with the ZnO colloidal solution aged for 30 min. The UV absorption and emission peaks at around 320 nm and 380 nm in Figure 4.1, respectively, indicate that ZnO nanoparticles were successfully synthesized via this new method. Here it should be noted that the green emission at around 500 nm originated from the oxygen vacancies on the ZnO nanoparticle surface. In addition, the colloidal ZnO nanoparticle solution shows a wide range of absorption properties as particles grow in size during the aging time, termed quantum confinement effect. Figure 4.2 demonstrates the red shifts of UV-Vis absorption peaks in response to the expanded aging time accompanying the growth of ZnO nanoparticles in size.

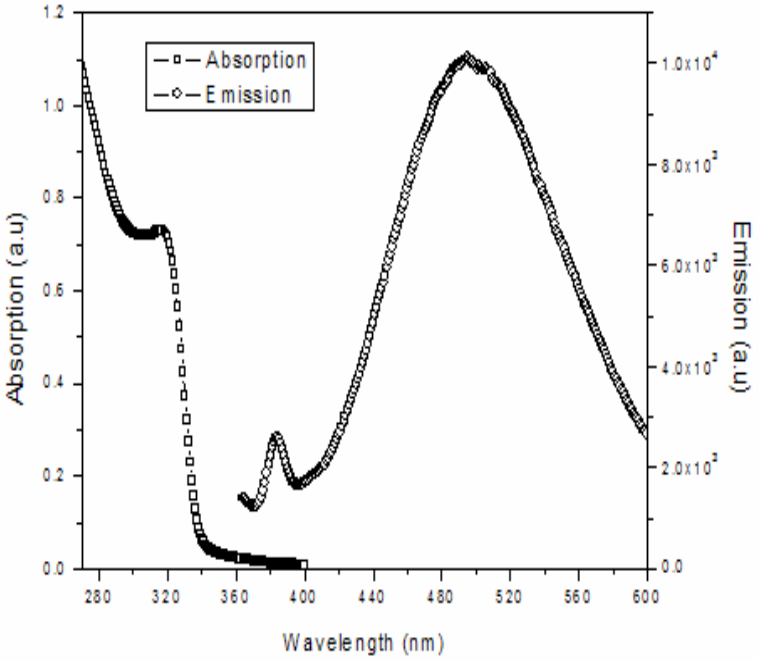

Figure 4.1. Photoluminescence and UV-Vis spectra of the ZnO nanoparticles aged for 30 min at 55 °C.

4.2 Size analysis of ZnO nanoparticles

There are several methods to measure nanoparticle sizes, including TEM imaging, small angle X-ray scattering (SAXS) and the Debye-Scherer formula which uses the width of the peak at half of its maximum (FWHM) height of the wide angle X-ray scattering.

In this work the UV-Vis absorption spectra in Figure 4.2 was used to calculate the nanoparticle sizes. This method was proposed by Meulenkamp who introduced the equation below which correlates the particle sizes to $\lambda_{1/2}$ (the wavelength at which the absorption becomes half of that at the shoulder) [10]. The values of 2.4 nm and 3.7 nm for the diameters of the ZnO samples which were aged for 10 min and 24 hours, respectively, were calculated from this equation.

$$1240/\lambda_{1/2} = a + b/D^2 - c/D,$$

where,

$a = 3.301$, $b = 294.0$ and $c = -1.09$,

$\lambda_{1/2}$ (nm) is the wavelength at which the absorption becomes half of that at the shoulder,

D (Å) is the diameter of the particles.

To confirm the particle sizes calculated from the equation above, the particle sizes were directly measured from TEM images of the ZnO nanoparticles aged for 3 hours. The

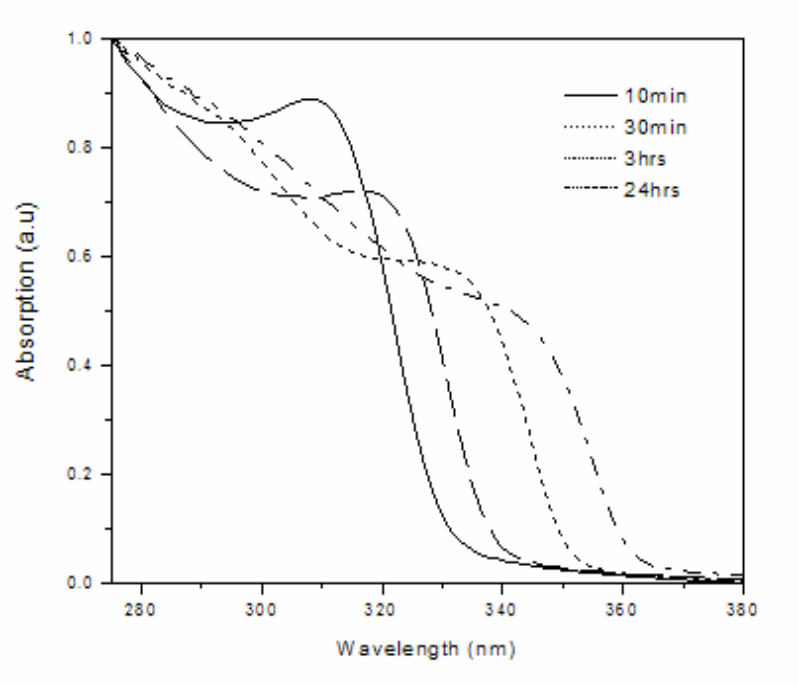

Figure 4.2. The red shifts of UV-Vis absorption peaks in response to the expanded aging time accompanying the growth of ZnO nanoparticles in size.

average particles size of ~ 3.5 nm was obtained from the TEM images (Fig 4.3), while the value of ~ 3.4 nm was calculated upon utilizing the equation above with the same particles. This shows a good agreement between the results from the two methods. In addition, the size growth about up to 5 nm was recorded when ZnO nanoparticles were aged for long time via this method.

4.3 Intermediate states between the colloidal and powder ZnO

The transparent ZnO colloidal solution turned to be cloudy after two-day aging under stirring and refluxing at 55 °C, followed by the precipitation of white powders onto the bottom of the glass flask. The white precipitants were treated under several different ways described in the experimental section in detail in order to study the effects of post-synthesis treatments on the characterizations of nanoparticles. Both XRD and TEM results revealed that the structures and morphologies can be affected by the surface environments, depending on how the white precipitants were prepared.

4.3.1 Effects of drying conditions of white precipitants

As already shown in the previous section, the UV-Vis, PL spectra and TEM image confirmed that spherical ZnO nanoparticles in the size range of about 2.5 to 5 nm were synthesized in the transparent methanol solution. However, an unknown material having a totally different structure in comparison to wurzite structure ZnO was observed from

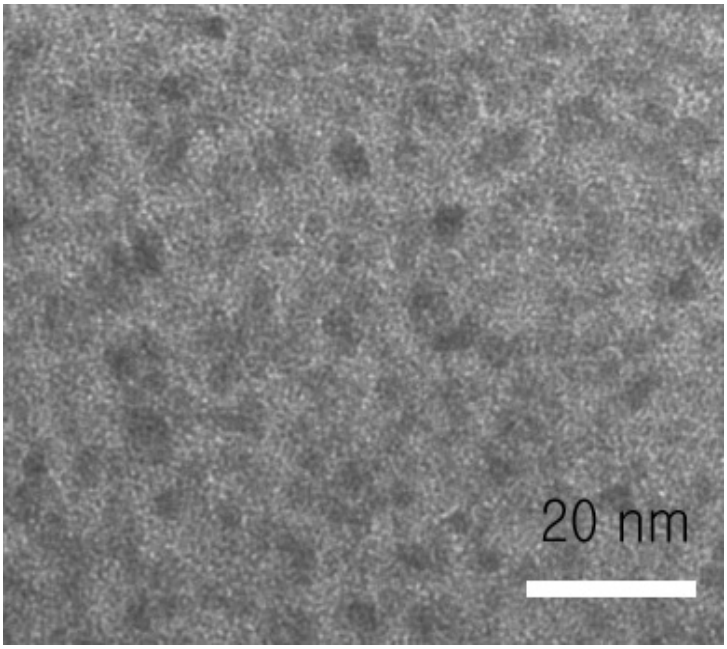

Figure 4.3. TEM image of the transparent colloidal ZnO nanoparticles aged for 3 hours.

the XRD when the white powder sample was prepared via the slow MeOH volatilization (Fig. 4.4). The XRD was run again with other sample in which methanol was quickly evaporated within 1 day. Figure 4.5 shows the result that the three main characteristic peaks of the wurzite structure of ZnO appeared again. However, when the sample above was not completely dried and placed several days in the open air at room temperature, probably due to the humidity in air, characteristic peaks from the both Fig. 4.4 and 4.5 appeared together in Figure 4.6. In addition, when XRD was taken after one month with the same sample, the peak intensity in Fig. 4.6 reduced and the intensity of the unknown peaks in Fig. 4.4 significantly increased again (Fig. 4.7) This finding indicates that there was a change in the structure of ZnO during the sample treatments due to the changes in surface environments of the particles. To minimize the time of MeOH evaporation as well as exposure to atmosphere during the sample preparation, the white powder was taken for XRD right after centrifuging and decantation of the opaque ZnO colloidal solution. The result coincided with what was shown in the quickly evaporated ZnO sample (Fig. 4.4), indicating the change in structures is attributed to the interactions between the slow removal of methanol solvents and humidity on the particle surface. The excess KOH remained on the particles surface after synthesis and may react with the humidity during the slow MeOH volatilization, resulting in the structural change. KOH is well known as a moisture sensitive material and its characteristic peak of the XRD also appears around at 33.2 °C. It has also been reported that adsorption and removal of the solvents can affect the structural change of ZnS nanoparticles [29].

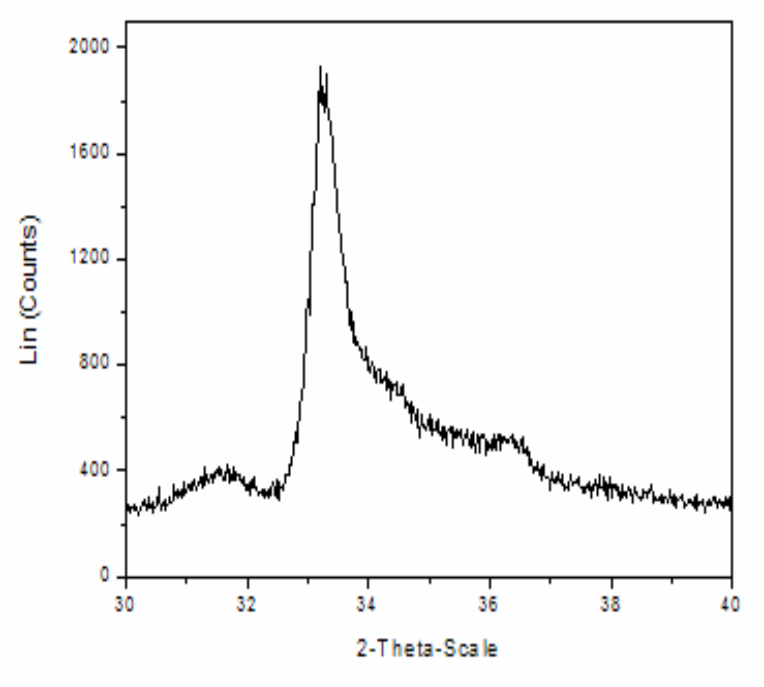

Figure 4.4. XRD pattern of the white precipitants. The powder sample was prepared via the slow MeOH volatilization method.

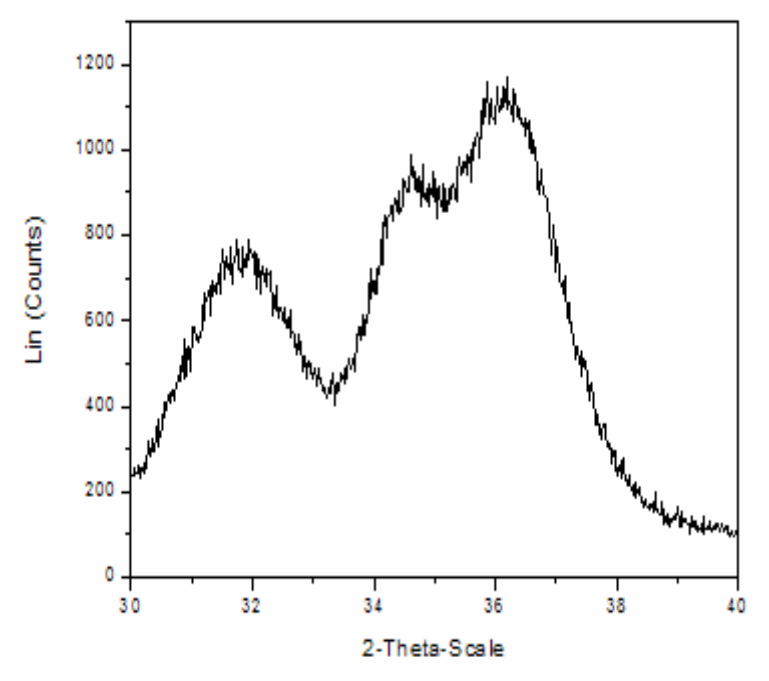

Figure 4.5. XRD pattern of the white precipitants showing three main characteristic peaks of the wurzite structure of ZnO. The powder sample was prepared by quick MeOH volatilization.

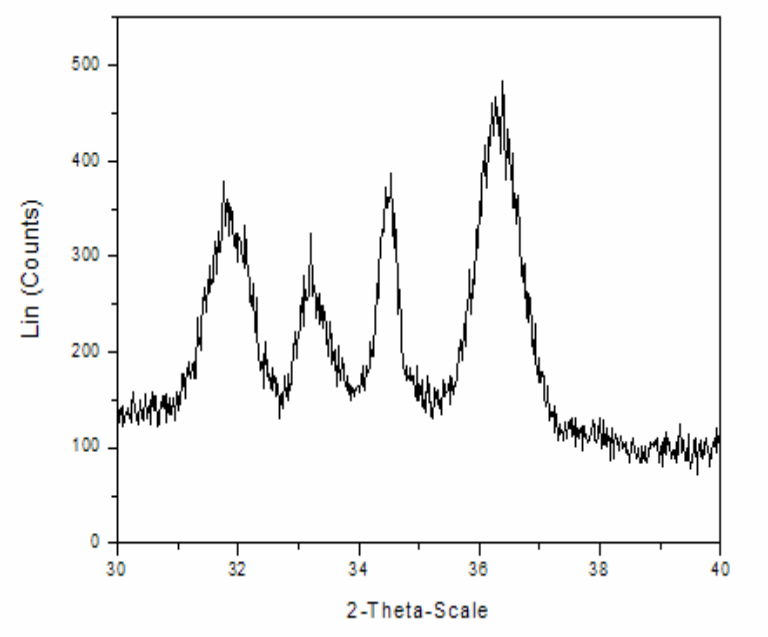

Figure 4.6. XRD pattern of the white precipitants showing both wurzite structure of ZnO peaks and peaks in Fig. 4.4. The powder sample was prepared by quick MeOH volatilization but the sample is still wetted with moisture.

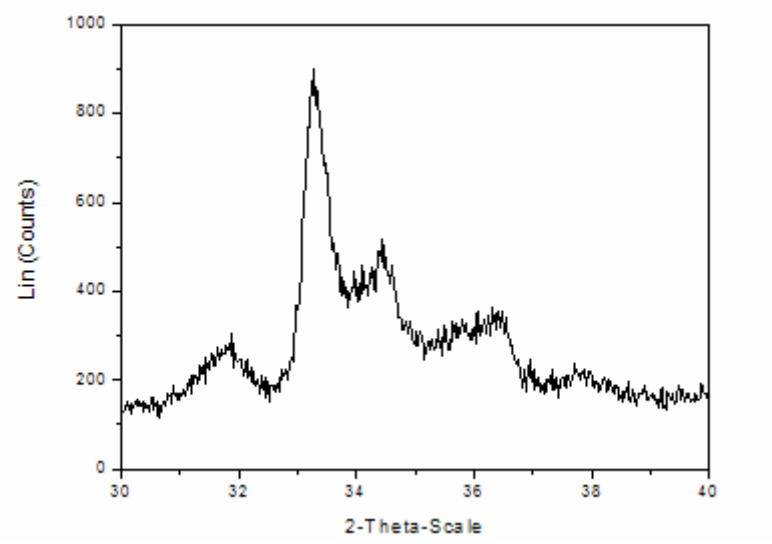

Figure 4.7. XRD pattern of the white precipitant. The sample was prepared in the same way used in Fig. 4.6 but placed to open air for one month to observe further structural changes in a humid atmosphere.

4.3.2 Effects of annealing

To identify the unknown white material, both TEM and XRD were utilized with the powder annealed for different lengths of time (30 min, 1 hr, 3 hrs) at 130 °C. Both TEM image and XRD pattern in Fig (4.8) were taken from the unknown sample, corresponding to XRD pattern in Fig (4.4). Before annealed, a flexible and spacious sheet-like material rather than spherical ZnO nanoparticles was observed. At the beginning of the annealing, however, the large area covered with the unknown material started to decrease and particles began to form (Fig. 4.9 (a)). This finding coincides with the corresponding XRD result showing that the peak at 33.2 ° is still predominant but the three main characteristic peaks of the wurzite structure ZnO begin to appear (Fig.4.9 (b)). When annealed for 1 hour, the peak at 33.2 ° was completely disappeared and only specific peaks of the wurzite structure of ZnO were shown on the XRD in Fig (4.10 (b)). The TEM image in Fig (4.10 (a)) also shows a good agreement with the result in XRD pattern. According to the TEM image, only ZnO particles are remained. However, both the shape and size of ZnO nanoparticles are not still uniform. After 3 hours annealing of the unknown precipitant,, spherical and uniform size still below 10 nm ZnO nanoparticles were obtained (Fig. 4.11 (a)).

The re-formation of ZnO nanoparticles after annealing the unknown materials is thought to be due to the heat decompositions of the hydrozincite or zinc hydroxide at the high temperature. The equation of chemical reaction is provided as following;

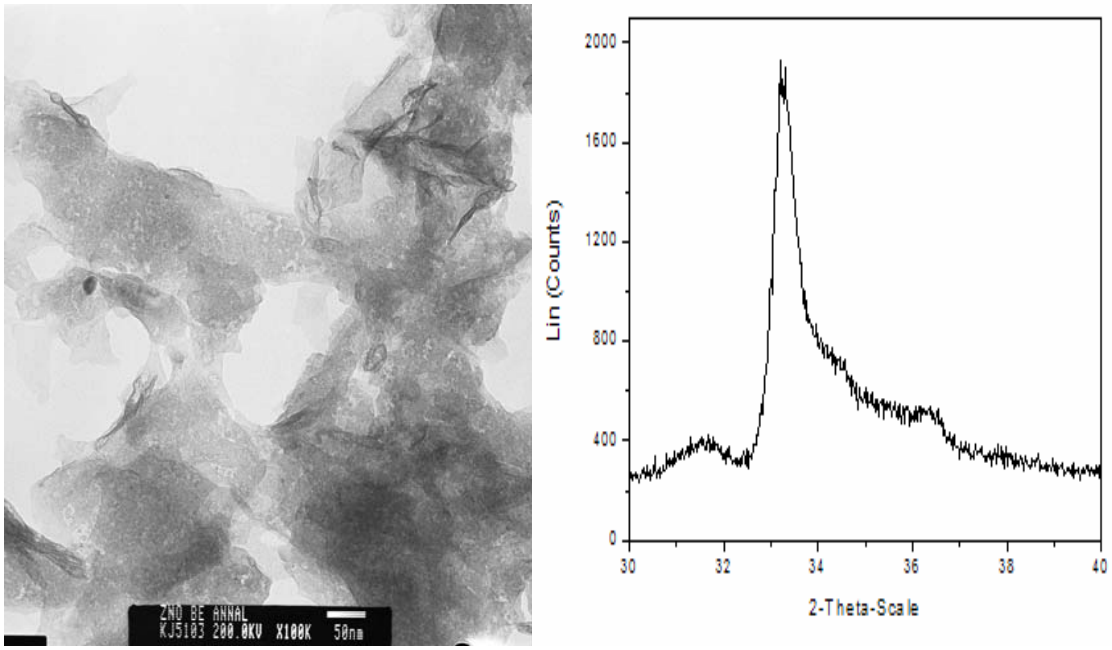

(a) (b)

Figure 4.8. TEM image (a) and XRD pattern (b) of sample (b-1) before annealing.

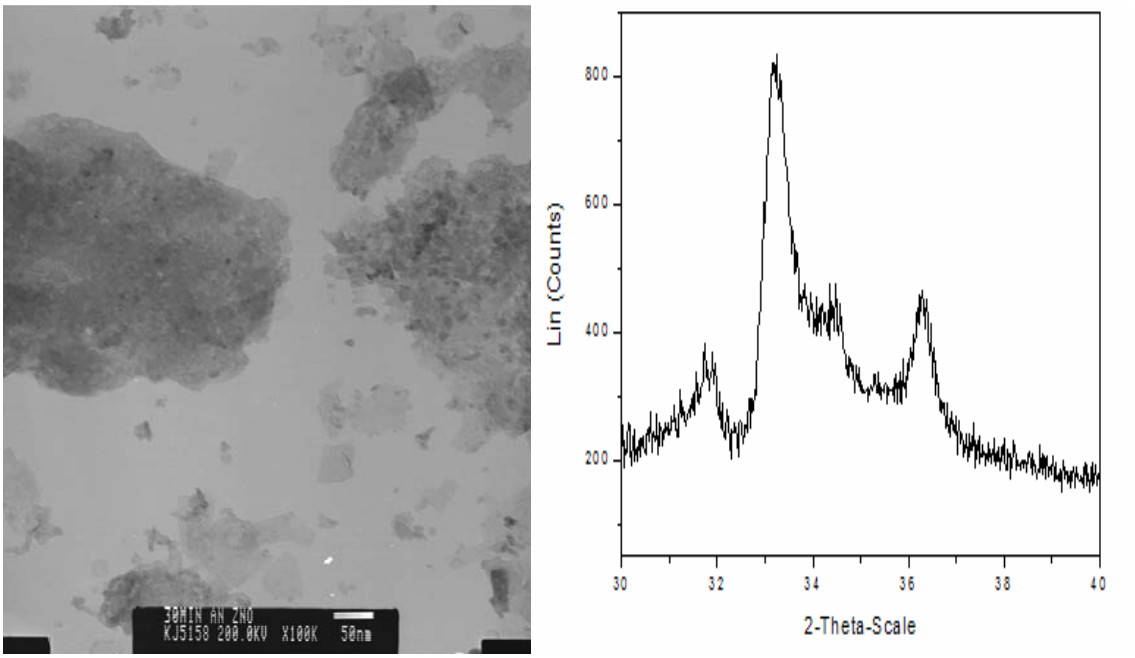

(a) (b)

Figure 4.9. TEM image (a) and XRD pattern (b) of sample (b-1) annealed for 30 min at 130 °C.

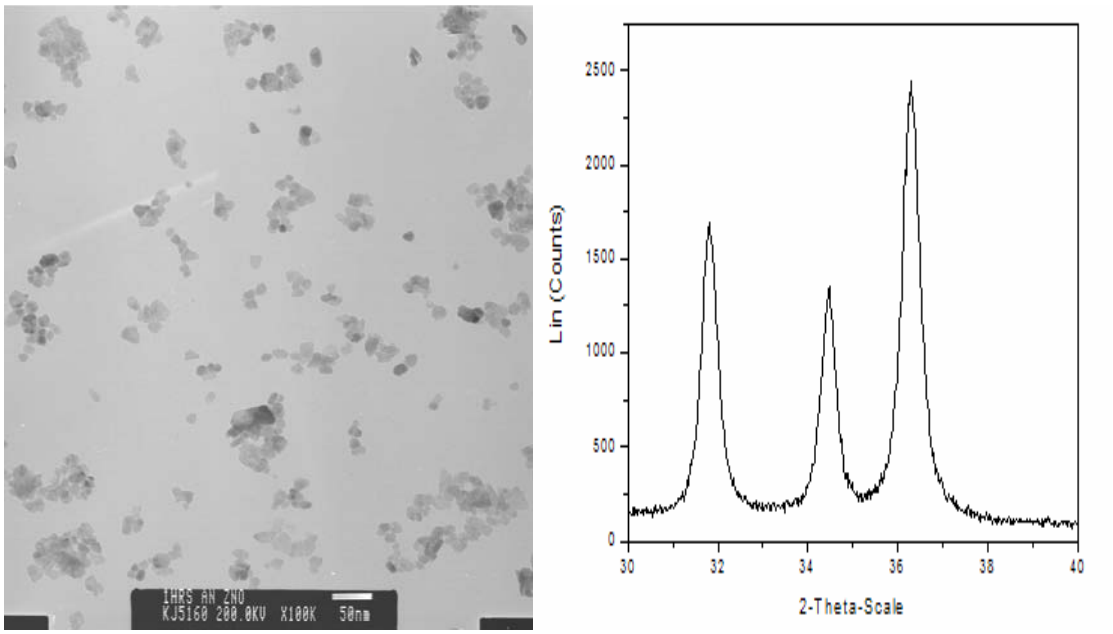

(a) (b)

Figure 4.10. (a) TEM image (a) and XRD pattern (b) of sample (b-1) annealed for 1 hour at 130 °C.

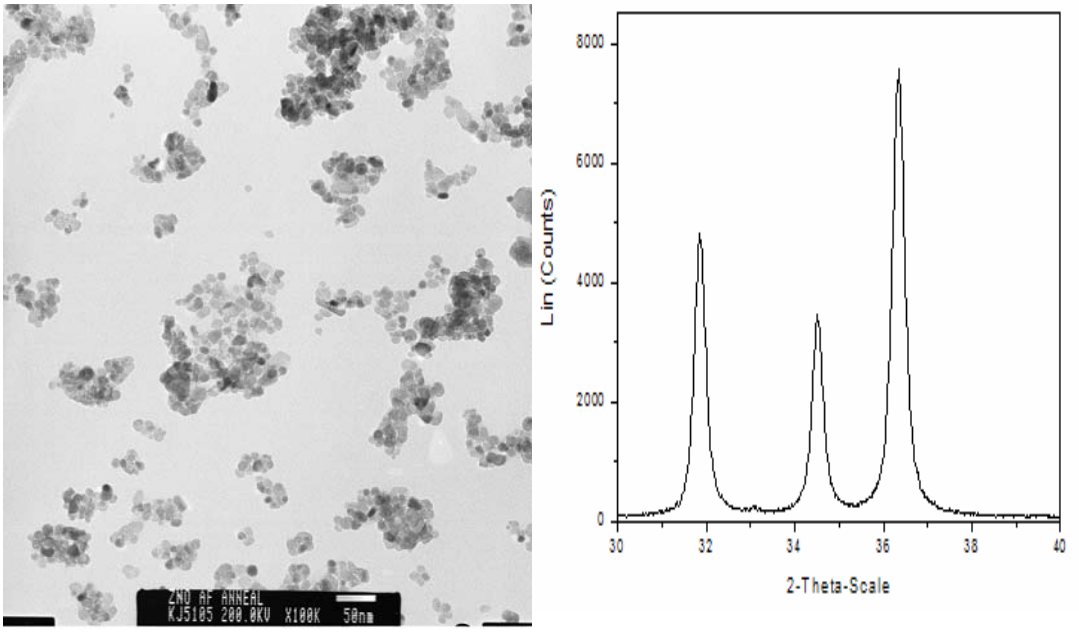

(a) (b)

Figure 4.11. TEM image (a) and XRD pattern (b) of sample (b-1) annealed for 3 hours at 130 °C.

- Hydrozincite: $Zn_5(OH)_6(CO_3)_2 \rightarrow 5ZnO+3H_2O+2CO_2$
- Zinc Hydroxide: $Zn(OH)_2 \rightarrow ZnO+H_2O$

In addition, the XRD peak analysis of the unknown materials also reveals that the specific peak of the unknown material at around 33.2 ° coincides with that of the hydrozincite or zinc hydroxide (or the mixture of them).

4.3.3 Other parameters

It has been reported that the water binding on the ZnS nanoparticle surfaces can cause the change in its structure [29]. To study the effect of water binding on the ZnO nanoparticle surface, distilled water was added to the opaque ZnO colloidal solution and ZnO powder obtained after 3-hour annealing, respectively. Furthermore, the pH values of the ZnO colloidal solution before and after adding distilled water were recorded. No changes in structures were observed from the both water added colloidal and solid state ZnO nanoparticles from the XRD. In addition, the pH values of each solution also recorded similar value.

Reversible surface-controlled structure transformation by the changes in the aggregation state and methanol desorption was also reported [28, 29]. To observe whether the reversible structure transformation occurs or not in our system, the methanol was added to the 3 hours annealed ZnO nanoparticle powder and the mixture was placed at room

temperature for 3 days. The XRD result shows that there is no difference between the two.

4.4 Summary

In summary, ZnO colloidal nanoparticles were successfully synthesized via our new wet-chemistry approach, confirmed by both UV-Vis, PL spectra and TEM image. The particle size in the range of about 2.5 to 5 nm was observed, calculated by using the UV-Vis absorption spectra and directly measured from the TEM images.

The changes in structures of the ZnO were found after slow removal of methanol solvent, resulting in an occurrence of the unknown material. It is thought that excess KOH on the particle surface plays an important role in the structural changes in open air during the slow volatilization of methanol solvent. The XRD peak analysis of the result material indicates that it may be the hydrozincite and zinc hydroxide.

The annealing process allowed the reversible structural transformation from the unknown material to wurzite structure of ZnO. This can be explained by the heat decomposition of the hydrozincite/ zinc hydroxide at a high temperature. No structural changes of the particles were observed by other surface environments such as water binding, pH change, re-absorption of methanol. All the experimental procedures and results were schematically summarized in Figure 4.12.

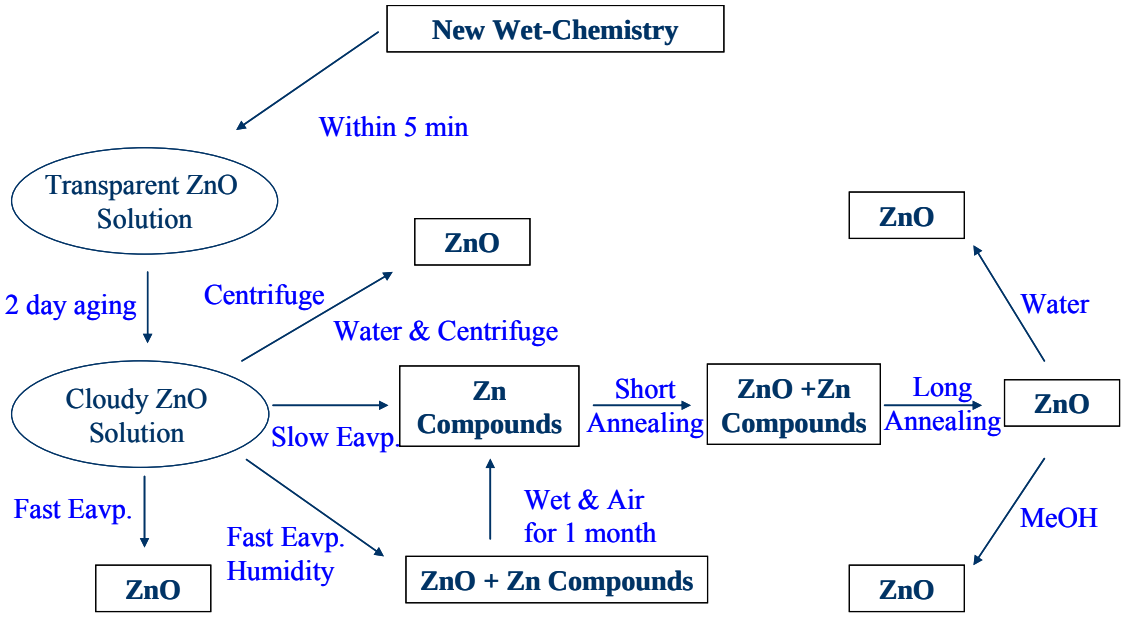

Figure 4.12 Schematic diagram showing all the experimental procedures and results of the stability of ZnO nanoparticles under different surface environments.

5. GROWTH MECHANISMS OF COLLOIDAL ZnO NANORODS

5.1 Formations of narrow and uniform ZnO nanorods

Based on the above precursor solution, ZnO nanorods were prepared using two approaches to achieve higher concentrations. As shown in Figs. 5.1(a) and 5.2(a), when the ZnO nanorods are prepared by increasing the concentration of the precursor solution by five times from 0.02 to 0.1 M using a Rotavapor and aged for 12 hrs under refluxing and stirring at 55 °C, highly uniform nanorods with diameters of about 5 nm are formed. When ZnO nanorods are prepared by concentrating the precursor solution from 0.02 to 0.04 M via a 10-day aging at 55 °C and refluxing conditions with a small cap opening, as shown in Figs. 5.1(b) and 5.2(d), again, highly uniform nanorods with diameters of about 5 nm are formed. However, if the concentration is below 0.04 M, no nanorods can be found. It should be noted that the Rotacapor evaporation approach leads to low reproducibility, requiring further research.

It is noted that the ZnO nanorods obtained from both of the above two approaches show high uniformity as well as small diameters of nanorods (~5 nm), with an aspect ratio of about 10 (Figs. 5.1 and 5.2). This result suggests that the wet chemistry carried out in this study yields unique ZnO nanorods growth mechanisms. Unlike what has been reported in the literature [34], the quasi-spherical ZnO nanoparticles prepared here stay at about 5 nm in size and do not grow further in size even after prolonged aging. The

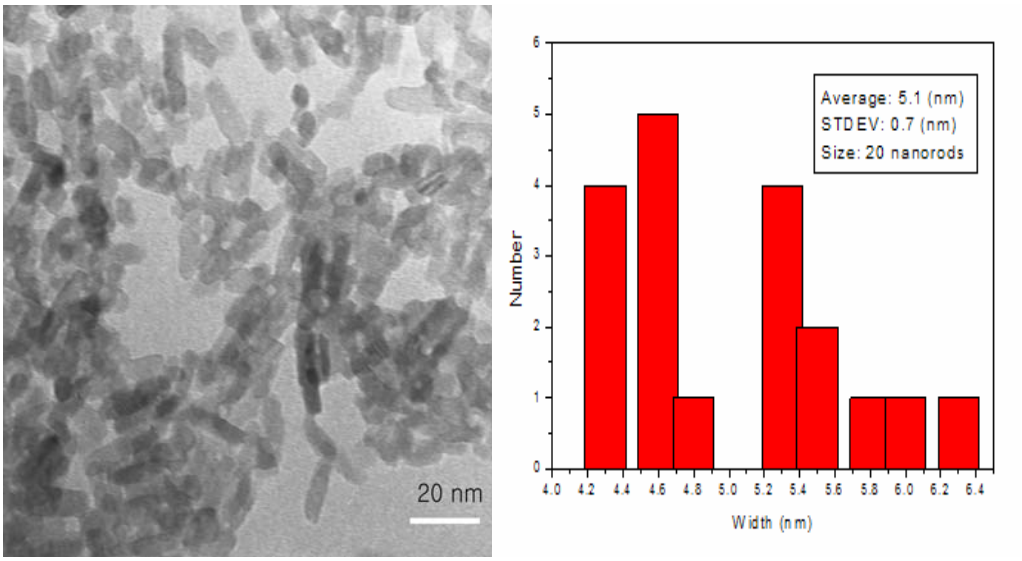

(a) (b)

Figure 5.1. TEM of ZnO nanorods grown when the starting solution was concentrated rapidly using a rotary evaporator (a). The graph (b) describes the average size and size distribution of ZnO nanorods shown in (a).

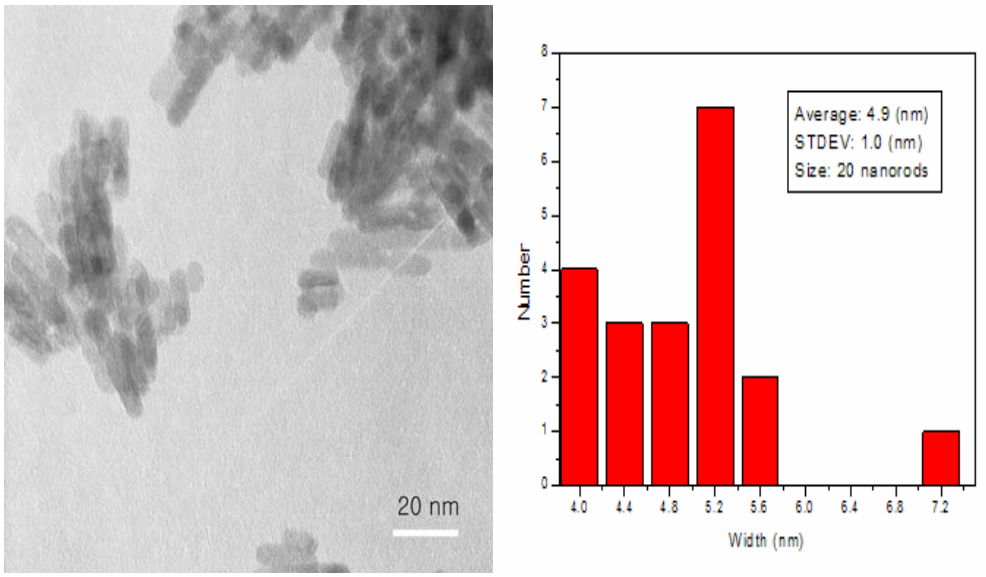

(a) (b)

Figure 5.2. TEM of ZnO nanorods grown when the starting solution was concentrated slowly with a loosely capped opening (a). The graph (b) describes the average size and size distribution of ZnO nanorods shown in (a).

critical concentration for the inception of nanorods formation based on the new wet chemistry approach is also much lower than what has been reported in the literature [32]. At this moment, it is still uncertain exactly why and how the new wet chemistry leads to the unique formation of ZnO nanorods. It can be speculated that the new wet chemistry approach allows for effective acetate ligand bonding on the particle surface to control the size and shape growth of ZnO nanocrystal via a closely packed monolayer of the coordinating acetate ligands. It has been reported that surfactant ligands can affect the size and shape growth of nanocrystals [23].

For the nanorods to form, it requires anisotropic crystal growth which depends on the differences in free surface energies on different crystallographic planes [32]. In this case, selective bonding of surface acetate ligands to the respective crystallographic planes allows the quasi-spherical nanocrystals to grow preferentially along the c-axis (002) of the wurtzite structure, making this axis the long axis of the rods [35]. A similar discussion concerning the role of counter-ion adsorption for crystal growth during biomineralization of rhombohedral calcite crystals has also been reported [36].

5.2 Study of structure and growth mechanisms of ZnO nanorods

5.2.1 Oriented attachment and High Resolution TEM

To study the structure and growth mechanisms of ZnO nanorods, HRTEM was taken by sampling the ZnO during the intermediate growth process from the reactor under various time frames. Figure 5.3 shows the HRTEM images of the ZnO at various stages of growth. HRTEM images show that the crystalline lattice planes of nanoparticles with sizes of 4-5 nm were almost perfectly aligned when joined. This phenomenon is called "oriented attachment" [37], which is a recent model proposed by Penn and Banfield to describe the crystal growth of anatase and iron oxide nanoparticles with sizes of a few nanometers. Therefore, the growth of ZnO nanorods along the c-axis is possibly resulted from both the acetate ligands, which help bond ZnO crystals selectively to grow ZnO nanorods from a preferred c-axis crystallographic plane, and oriented attachment of perfectly aligned lattice planes [33].

5.2.2 Quantum confinement effect and UV-Vis absorption

UV-Vis absorption spectra of both ZnO nanoparticles and nanorods are shown in Figure 5.4. In most cases, quantum confinement effects from the optically active nanorods semiconductors are not shown due to their large rod diameters [38-41]. Peng, et al. [42], however, first noticed quantum confinement effect on small dimensions CdSe quantum

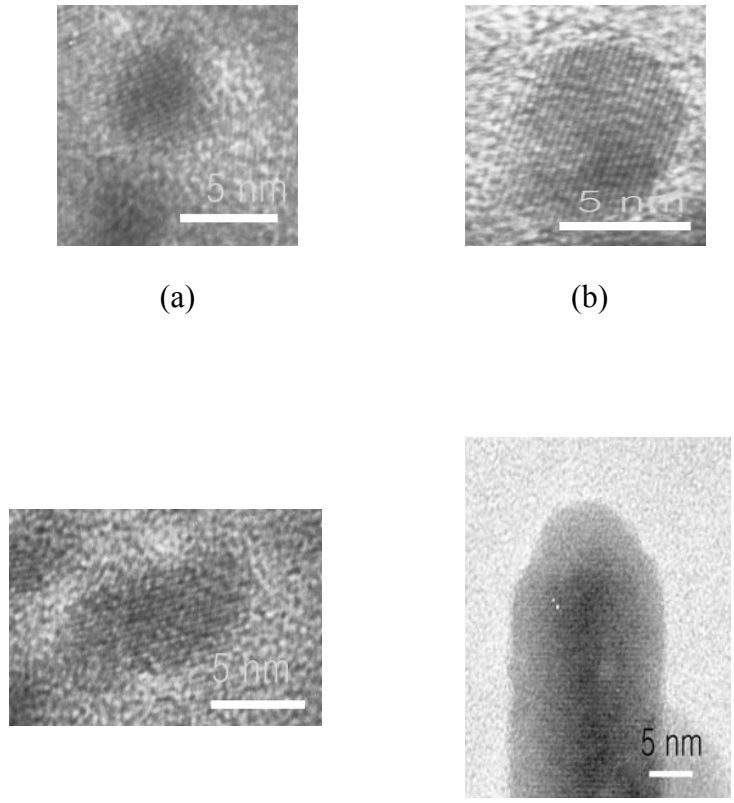

(a) (b)

(c) (d)

Figure 5.3. HRTEM shows perfectly aligned crystalline lattice planes of ZnO nanocrystals in (a) one, (b) joining of two, (c) joining of three nanoparticles. In (d), the fully grown ZnO nanorod after annealing is shown.

rods, where red shift of the PL peak of a CdSe quantum rod was observed. The mechanism for UV absorption below 380 nm in bulk ZnO materials is known as bandgap absorption; while the shifts observed on UV absorption in ZnO nanocrystals are due to their changes in size within the quantum confinement regime [34]. It has been reported that ZnO shows quantum confinement effects for particles below 7 nm in size [43]. Fig. 5.4 shows a similar quantum confinement effect on the 5 nm diameter ZnO nanorods. ZnO nanorods after being aged for 10 days have a rod diameter of 5 nm and still show the red shift. For ZnO nanorods being aged for 15 days, it has a diameter of 11 nm. The observed UV-Vis absorption spectrum for the 11 nm nanorods is almost the same as that of the bulk ZnO. The absorption observed above 380 nm is believed to be due to the scattering of the incident beam on the opaque ZnO nanorod solution.

5.2.3 Structure of ZnO nanorods and diffraction mode TEM

Both electron diffraction and HRTEM confirm the ZnO rod morphology and structure (Figs. 5.1, 5.2 and 5.3). ZnO nanorods aged for 15 days *via* slow evaporation were prepared for TEM characterization (Fig. 5.5). The image shows that ZnO nanorods have ~11 nm in diameter and a maximum aspect ratio of 6. The insets in Figs. 5.5(b) and 5.5(c) show the diffraction patterns of the selected ZnO nanorods. The hexagonal diffraction pattern in Fig. 5.5(b) corresponds to the (002) direction of the wurtzite ZnO nanorod, which is parallel to the beam direction. This hexagonally ordered diffraction pattern is not shown in Fig. 5.5(c) because most ZnO nanorods are oriented in an angle

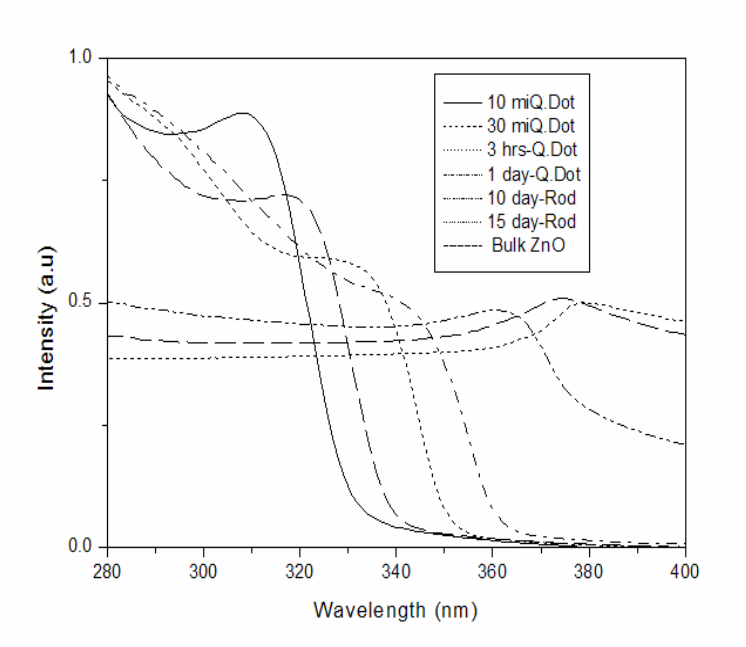

Figure 5.4. UV-Vis absorbance spectra of ZnO quantum dots and nanorods prepared under different aging times. It clearly shows the quantum confinement effect, shifts of the UV absorbance peaks.

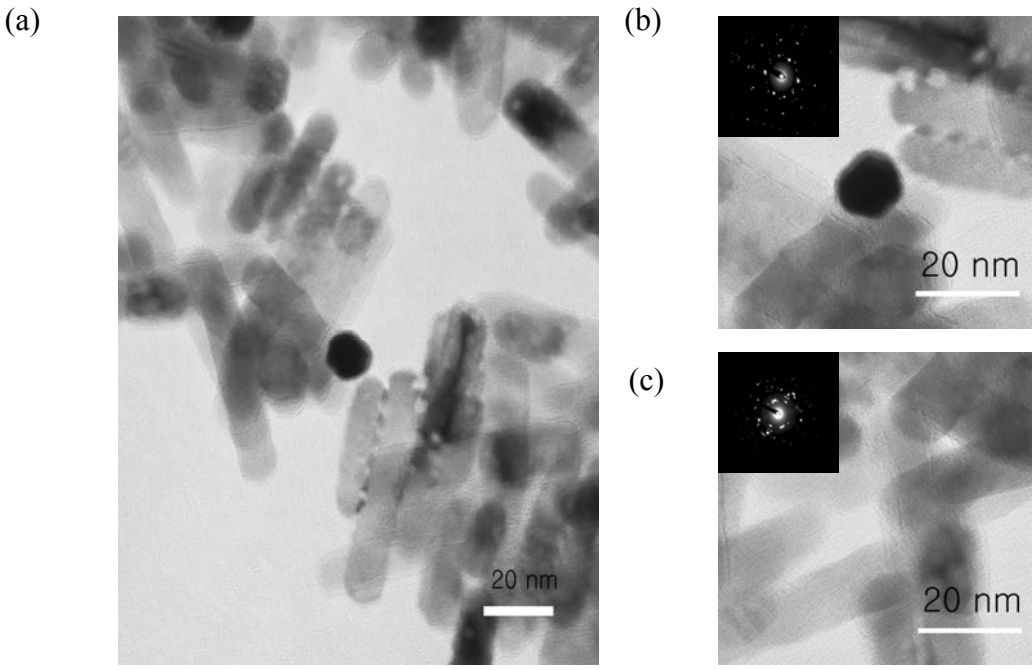

Figure 5.5. TEM of ZnO nanorods prepared after aging for 15 days. The insets in (b) and (c) represent the diffraction pattern of each selected crystal.

from the electron beam direction.

5.2.4 Annealing effect on the growth of ZnO and size analysis

To study the annealing effects on the further growth of ZnO nanorods, ZnO nanorods were prepared in the same way described above and then dried at 110°C for 3 hrs in a vacuum oven. The TEM images of ZnO nanorods before and after annealing are shown in Figs. 5.6(a) and 5.6(b). The TEM micrographs clearly show that ZnO nanorods grow randomly in all directions during the annealing, leading to a wider distribution of ZnO nanorods both in diameter and in aspect ratio. The average diameters of ZnO nanorod before and after annealing are about 6.2 and 12.2 nm, respectively. This increase in diameter is thought to be the result of the intra- or inter-atom diffusions of ZnO nanorods promoted by the temperature rise.

The corresponding XRD diffraction patterns of ZnO nanorods are shown in Figs. 5.7(a) and 5.7(b). Compared to the XRD pattern of wurtzite structure of ZnO nanoparticles elsewhere, the same XRD peaks are observed, except for a much higher relative peak along the c-axis for the ZnO nanorods. This indicates that ZnO nanorods are well grown in the (002) direction. Furthermore, much narrower peak widths as well as reduced background intensity of the XRD patterns reveal that a much higher degree of crystallinity of wurtzite structure of ZnO nanorods is obtained after annealing the powder samples for 3 hours at 110 °C in a vacuum oven.

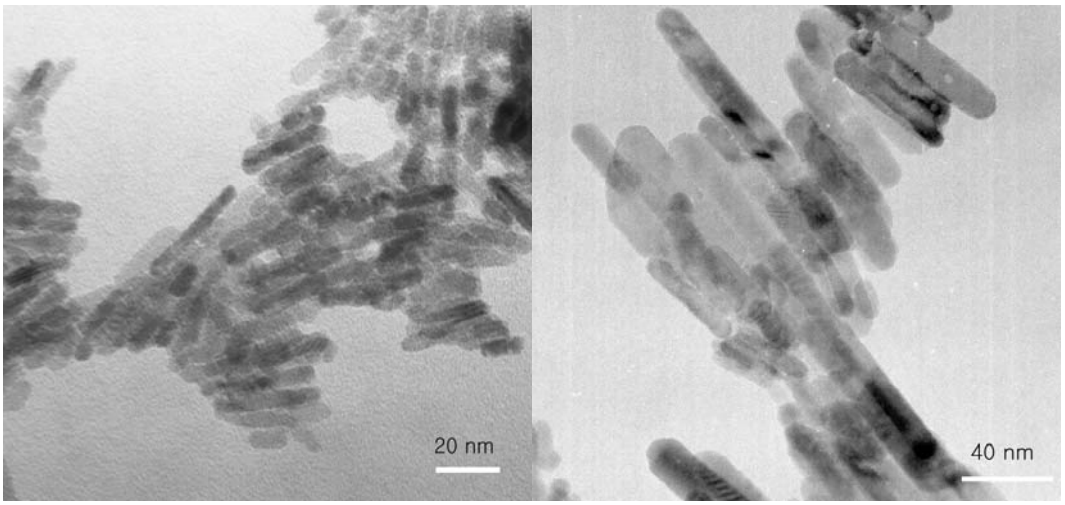

(a) (b)

Figure 5.6. TEM of the ZnO nanorods before (a) and after (b) annealing at 110℃ for 3 hrs.

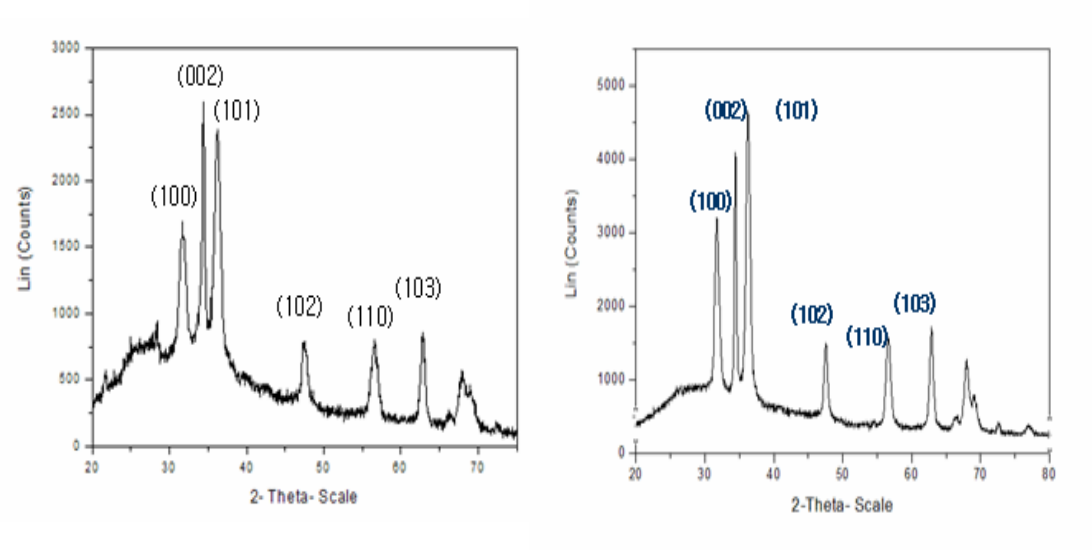

(a) (b)

Figure 5.7**.** XRD of the ZnO nanorods before (a) and after (b) annealing at 110℃ for 3 hrs corresponding to TEM in Fig. 5.6 (a) and (b), respectively.

The width of ZnO nanorods can be calculated based on the peak width of the XRD peaks using the Debye-Scherer formula, $t = 0.89\lambda/(\beta\cos\theta_B)$, where λ is the X-ray wavelength (1.5406 Å), θ_B is the Bragg diffraction angle, and β is the peak width at half-maximum. The diameters of 7.4 and 11.4 nm, respectively, are calculated for ZnO nanorods before and after annealing. These results are about 1 nm apart from the TEM images. This finding shows a good agreement between the XRD measurements using the Debye-Scherer formula and the TEM direct imaging.

5.2.5 Other factors on the ZnO nanorod formation

It should be noted that ZnO nanorods in the diameter of ~ 11 nm were also observed after aging for 17 days at 45°C. However, no nanorods can be found if the solution is aged at room temperature. These findings indicate that elevated temperature is needed to trigger atomic diffusion and phase transition for the formation of ZnO nanorods within a reasonable laboratory time scale. Nonetheless, aging time is a crucial factor to affect ZnO nanorod diameters.

5.3 Summary

In summary, three distinct growth stages are observed in the growth of ZnO from quantum dots to rods. At the early stage, the size of both nanoparticles and nanorods were confined to below 5 nm. This is thought to be due to the zinc acetate ligand

bonding on the particle surfaces, which prevents nanoparticles from growing further. Two different stages of growth mechanisms in the nanocrystal growth process were suggested: “focusing” and “defocusing’ stages [21]. During the focusing stage, the smaller particles grow faster than the larger ones, and as a result, the size distribution can be focused down to one that is nearly monodisperse. However, in defocusing stage (Ostwald ripening), small nanocrystals are depleted as larger ones grow bigger and the size distribution broadens, or defocuses. Therefore, it is apparent that the growth of narrowly dispersed spherical ZnO nanocrystals at the early stage is in the “focusing” stage.

At the intermediate stage, ZnO nanorods are grown along the c-axis of the wurtzite structure. The highest aspect ratio of ZnO nanorods is found at this stage. This is resulted from the oriented attachment and selective bonding of zinc acetate ligands to the respective crystallographic planes, allowing spherical nanocrystals to grow preferentially along the c-axis, making this axis the long axis of the rods.

At the last stage, nanorods grow simultaneously in all directions, leading to the decrease in aspect ratio. This finding is consistent with the defocusing model (Ostwald ripening) introduced previously.

6. CONCLUSION

The characteristics of ZnO colloidal nanoparticles synthesized via our new wet-chemistry approach were studied by using an UV-Vis spectrophotometer, PL, XRD and TEM. The particle size in the range of about 2.5 to 5 nm was obtained from the both the UV-Vis absorption spectra and the TEM images. Structural transformations were observed from the white precipitants in ZnO colloidal solution. Slow volatilization of MeOH and excess KOH on the particle surface cause changes in structures. The XRD peak analysis indicated that the precipitant may be the hydrozincite and zinc hydroxide, supported by the reaction equation during the annealing. No structural changes were observed by other surface environments such as water binding, pH change, re-absorption of methanol.

HRTEM, electron diffraction and XRD have been used to study the morphology, structure, size and shape evolution of the ZnO nanocrystals. Wurtzite ZnO nanorods having small diameters and narrow size distribution have been grown using our unique wet-chemistry at a much lower concentration than expected. Three distinct nanorod growth stages are observed: 1) formation of quasi-spherical nanoparticles with diameters < 5 nm, 2) preferential growth of ZnO nanorods along the c-axis, and 3) random growth of ZnO nanoparticles in all directions. Important processing parameters for the formation of ZnO nanorods, such as temperature, concentration of solution, annealing,

and aging time, were also studied. It is observed that the diameter of ZnO nanorods is only sensitive to aging time, not the temperature of reaction.

REFERENCES

(1) Lieber, C. M. *Solid State Commun*. **1998**, *107*, 607-616

(2) Smalley, R. E.; Yakobson, B. I. *Solid State Commun*. **1998**, *107*, 597-606

(3) Edelstein, A.S.; Cammarata, R.C. *Nanomaterials:*, *Synthesis, Properties and Applications*, (Edelstein, Ed). Institute of Physics Publishing: Bristol, UK **1996**

(4) O'Regan. B.; Gratzel, M.; *Nature* **1991**, *353*, 737-740

(5) Colvin, V.L.; Schlamp, M.C.; Aliviastos, A.P.; *Nature* **1994**, *370*, 354-357

(6) Koch, U. *A.Chem. Phys. Lett*. **1985**, *122*, 507-510

(7) Muthukumar, S.; Sheng, H.; Zhong. J; Zhang, Z.; Ematetoglu, N.W.; Yicheng, L.; *Nanotechnology, IEEE* Mar **2003**, *2*, 50-54

(8) Look, D. C.; *Mater. Sci. Eng B.* **2001**, *80*, 383-387

(9) Lee, W.; Jeong, M.-C.; Myoung, J.-M. *Nanotechnology* **2004,** *15*, 1441-1445

(10) Spanhel, L.; Anderson, M. *J. Am. Chem. Soc*. **1991**, *113*, 2826

(11) Nuth, J. A.; *Nature* **1987**, *329*. 589

(12) McHale, J. M.; Auroux, A.; Perrotta, A. J.; Navrotsky, A. *Science* **1997**, *277*, 788-791

(13) Li, Y.; Lee, K.-J.; Sue, H.-J.; Miyatake, N.; Nishimura, R. submitted to *J. Am. Chem. Soc,* **2005**

(14) Lee, K.-J.; Miyatake, N.; Wong, M.; Sue, H.-J; submitted to *Nano Letts.* **2005**.

(15) Borgohain, K.; Mahamuni, S. *Semicond. Sci. Technol*. **1998**. *13.* 1154-1157

(16) Zhou, H.; Alves, H.; Hofmann, D.M.; Meyer, B.K.; Kaczmarczyk. G.; Hoffmann,

A.; Thomsen, C. *Phys. Stat. sol (b)*. **2002**, *229*, 825-828

(17) Guo, L.; Yang, S.; Yang, C.; Yu, P.; Wang, J. Ge, W. Wong, G.K.L *Appl. Phys. Lett.* **2000**, *76*, 2901-2903

(18) Alexandre, M.; Dubois, P.; *Mater. Sci. Eng*. **2000**, *28*, 1-63

(19) Mcnaught, A.D; Wilkinson, A. *Compendium of Chemical Terminology*, 2nd Edition, Inter. Union of Pure and Appl. Chem. (IUPAC): Blackwell Science, UK **1997**

(20) Wendy, U. H.; Janke, J. D.; Alivisatos, A. P. *Science* **2002**, *295*, 2425-2427

(21) Peng, X.; Wickham, J.; Alivisatos, A. P. *J. Am. Chem. Soc*. **1998**, *120*, 5343-5344

(22) Peng, Z. A.; Peng, X. G. *J. Am. Chem. Soc*. **2001**, *123*, 1389-1395

(23) Puntes, V. P.; Krishnan, K. M.; Alivisatos, A. P. *Science* **2001**, *291*, 2115-2117

(24) Manna, L.; Scher, E. C.; Alivisatos, A. P. *J. Am. Chem. Soc*. **2000**, *122*, 12700-12706

(25) Flaschen, S. S.; *J. Am. Chem. Soc.* **1955**, *77*, 6194-6196

(26) Garvie, R. C. *J. Phys. Chem.* **1978**, *82*, 218-224

(27) Skandan, G.; Foster, C.M.; Frase, H.; Ali, M.N.; Parker, J.C.; Hahn, H. *Nanostruct. Mater*. **1992**, *1*, 313-322

(28) Huang, F.; Gilbert, B.; Zhang, H.; Banfield, J. F. *Phys. Rev. Lett*. **2004**, *92*, 155501

(29) Zhang, H.; Gilbert, B.; Huang, F.; Banfield, J. F. *Nature* **2003**, *424*, 1025-1029

(30) Bahnemann, D. W.; Kormann, C.; Hoffmann, M. R. *J. Phys. Chem*. **1987**, *91*, 3789-3798

(31) Meulenkamp, E. A.; *J. Phys. Chem. B*, **1998**, *102*, 5566-5572

(32) Pacholski, C.; Kornowski, A.; Weller, H. *Angew. Chem. Int. Ed*. **2002**, *41*, 7, 1188-1191

(33) Verges, M. A.; Mifsud, A.; Serna, C. J. *J. Chem. Soc. Faraday Trans*. **1990**, *86*, 959-963

(34) Meulenkamp, E. A. *J. Phys. Chem. B* **1998**, *102*, 5566-5572

(35) Yang, R. D.; Tripathy, S.; Li, Y.; Sue, H.-J. *Chem. Phys. Lett.* **2005**, *411*, 150-154

(36) Rajam, S.; Mann, S. J. *Chem. Soc. Chem. Commun*. **1990**, 1789-1791

(37) Penn. R. L.; Banfield, J. F. *Science* **1998**, *281*, 969-971

(38) Wang, W. Z. *Inorg. Chem. Commun*. **1999**, *2*, 83-85

(39) Han, W. ; Fan, S. ; Li, Q. ; Hu, Y. *Science* **1997**, *277*, 1287-1289

(40) Routkevitch, D.; Bigioni, T.; Moskovits, M.; Xu, J. M. *J. Phys. Chem*. **1996**, *100*, 14037-14047

(41) Trentler, T. J. ; Hickman, K. M. ; Goel, S. C. ; Viano, A. M. ; Gibbons, P. C. ; Buhro W. E. *Science* **1995**, *270*, 1791-1794

(42) Peng, X. ; Manna, L. ; Yang, W. ; Wickham, J. ; Scher, E. ; Kadavanich, A. ; Alivisatos, A. P. *Nature* **2000**, *404*, 59-61

(43) Koch, U.; Fojitik, A.; Weller, H.; Henglein, A. *Chem. Phys. Lett*. **1985**, *122*, 507-510

VITA

Kwang Jik Lee was born in Busan, South Korea where he had spent the most of his youth. He enrolled in the materials science and engineering program at Korea University in March 1995. After finishing military service for 30 months and with scholarships including first class honors during the schooling, he received his B.S degree in February 2002. Before enrolling in the Department of Mechanical Engineering at Texas A&M University in August 2003, he worked as a researcher in the Polymer Materials Lab of the Electronic Materials and Devices Research Center at the Korea Institute of Science and Technology (KIST). He received his M.S degree in mechanical engineering in August 2005. His permanent address is 39-40 Dae-yeon Dong, Nam-gu, Busan, South Korea.